Validation of Space Charge Laminar Flow in Diodes

Marco Cavenago*[1]
[1]INFN/LNL, Lab. Nazionali di Legnaro
*Corresponding author: v. Universitá 2, I-35020 Legnaro (PD) Italy, cavenago@lnl.infn.it

Abstract: Design of electron and ion diodes is the base of particle source extraction systems, and at least for small beam size or closed anode system may be approached with analytic techniques, validated before 1960 with analog computing. These design rules now offers us a known case against which to compare the precision of fluid and particle tracing codes. A laminar model for the particle flow is here used to show the need for introducing a thin strip between the ideal cathode position where the ruling Partial Differential Equation (PDE) is singular and the simulated cathode position; moreover condition for convergence of nonlinear solver are described. The effect of large anode lens aperture is computed with a moving mesh application, trying to determine aberrations due to finite aperture radius; a method for rapid convergence of trajectory and field calculation is here presented.

Keywords: diode, space charge, anode lens

1 Introduction

In the extraction and acceleration of a beam from a ion source or a thermionic emitter, the diode is the most simple building block and is common to all systems; as noted in fig 1 the anode is usually open and the diode is followed by other beam focusing systems[1, 2]. Closed anode may have some application for implantation, but they are mainly studied as a starting approximation for open anode system.

Importance of high current electron diodes in practical applications (power klystrons, to say one) has granted to this subject a considerable attention. Well above the capacity of available digital computers, diode design rules were developed before 1960 with a combination of analytic techniques for laminar flows [1, 3] and analog computing. Effects of source temperature are well understood[4] and typically less important of beam space charge. When the cathode size r_1 is small respect to the diode gap length d, defocussing effect of anode extraction hole is well understood[5], so that divergence of diode beam is correlated to its perveance $I/V_a^{3/2}$ with I and V_a the diode current and voltage[6, 7, 8, 9].

The quest for high H^- beam current, mainly for fusion application[10, 11] leads naturally to large r_1/d ratio for which design rules are not completely known[2]. Many digital computer codes now exist: precision of results poorly increases with the simulated number of particle trajectories. Most codes calculates space charge with a PIC (particle in cell) approach (or a ray map integration[12]) over a rectangular mesh, which is different from the FEM (finite element method) mesh, where fields are better computed. In this paper in order to match smoothly the FEM mesh to the beam, we will consider laminar beams only (see section 2) and use the Arbitrary Lagrangian Eulerian (ALE) application of Comsol Multiphysics.

In section 2 basic equation and the anode lens formula are recalled. Validation of the nonlinear numerical solver and its application to the known solution for closed anode system is discussed in section 3. Use of ALE modes and its application to a typical open anode ion diode is described in section 4, introducing a method of iterative beam solution, which is very rapidly converging in the case considered.

2 Basic equations and assumptions

A scheme of a typical diode extraction with two dimensional geometry is shown in 1, where z is the beam axis and x the trans-

verse direction; by assumption system is completely uniform in the coordinate y, that is in more physical words, the extension L_y in the y coordinates is much larger than the size L_x and L_y in the drawing plane zx. The magnetic field is neglected and motion is non relativistic. System is symmetric respect to the zy plane $x = 0$, so we draw only the $x \geq 0$ portion.

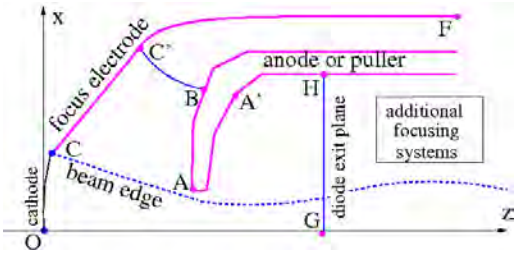

Figure 1: Scheme of typical diode extractor, zx section, with symmetry plane $x = 0$: the anode BAA' also called puller is supported by a tube at same potential; the emitting cathode OC is continued by a focus electrode $CC'F$; the open boundaries $C'B$ named gap and GH named exit plane delimits the simulation domain for the diode

Particles (say negative ions H^- to fix ideas) are emitted from a cathode with negligible speed (and temperature); cathode zx section is a circular arc, with radius R_1 and angular aperture $2\theta_c$; the angular coordinate θ spans the cathode. Since temperature is negligible the ion flow may be represented as laminar, that is, all ion at the same position have the same velocity; let (s, ℓ) be a curvilinear coordinate system following the flow lines and such as, at the idealized cathode position where ion have zero speed, we have $s = 0$ and $\ell = \theta$. The emitted current density $j_\parallel$ is parallel to flow lines, and we assume that it may depend on ℓ (say for effect of cathode heating), so that $j_e = j_\parallel(\ell)/j_\parallel(\theta_c)$ is the profile of the current. In other words $j_\parallel = -qj_a j_e(\ell)$ where j_a is a positive constant and current at cathode corner C is $-qj_a$.

We introduce the scaled potential $v = -q(\phi - \phi_C)/K_{E0}$ where ϕ is the usual electric potential, ϕ_C its value at ideal cathode and K_{E0} a reference energy given by

$$K_{E0} = |q| \left(|q| j_a {R_1}^2/k_0\right)^{2/3} \qquad (1)$$

$$k_0 = \frac{4\epsilon_0}{9}\sqrt{\frac{2|q|}{m}} \qquad (2)$$

with m and q the mass and (signed) charge of the particle, as usual.

The distance between two neighbor flow lines at $s = s_0$ be $\mathrm{d}\ell/\mathcal{G}(s_0, \ell)$; laminar flow assumption is valid where flow lines do not cross, that is $\mathcal{G}$ is bounded. Current density along a flow line is $j_\parallel(\ell)C(s, \ell)$ with the compression factor $C(s, \ell) = \mathcal{G}(s, \ell)/\mathcal{G}(0, \ell)$. In some context it is convenient to introduce the complex variables $z = z + ix$ and $w = s + i\ell$; let also $\triangle_z$ be the Laplacian in usual space coordinates, while $\triangle_w = \partial_s^2 + \partial_\ell^2$ is an operator in the w plane. For conformal transform $w(z)$ we note $|w_{,z}|^2 \triangle_z v = \triangle_w v$ and $\mathcal{G} = |w_{,z}|$.

Since charge density is $\rho = j/|\dot{z}|$ and the speed is $|\dot{z}| = (2K_{E0}v/m)^{1/2}$ in non relativistic approximation, the Poisson eq. $\triangle_z \phi = -\rho/\epsilon_0$ becomes

$$\triangle_z v = \frac{4}{9\sqrt{v}} \frac{j_e(\ell)}{R_1^2} C(s, \ell) \qquad (3)$$

2.1 The line converging flow

The line converging flow[3] is simply specified by $j_e = 1$ and the conformal transform

$$w \equiv s + i\ell = -\log\left(1 - \frac{z}{R_1}\right) \qquad (4)$$

whose inverse function $w^{(-1)}(w)$ is $z(w) = R_1(1 - \exp(-w))$. Equation 3 simplifies to

$$v_{,ss} = \tfrac{4}{9}\mathrm{e}^{-s} v^{-1/2} \qquad (5)$$

whose well known analytical solution for v is

$$v_r = s^{4/3}(1 - \tfrac{2}{15}s + \tfrac{11}{450}s^2 - \tfrac{437}{111375}s^3 + O(s^4)) \qquad (6)$$

It is possible to design[1] a diode (with closed anode) so that $v = v_r(s)$ and $j_e = 1$ holds exactly for $|\ell| \leq \theta_c$ (called beam region) and to use this diode as a validation example for numerical tools.

To fix ideas anode potential be v_a (of order unity) while v_ϵ is the real cathode potential (not exactly zero, but a very small quantity, say 10^{-4} or less). In the beam region, see fig 2, anode is simply $s = s_a$ with $v_a(s_a) = v_a$; this implies that anode has constant curvature radius $R_a = R_1(1 - \mathrm{e}^{-s_a})$; for example $v_a = 0.499$, $s_a = 0.630$ and $r_a = R_a/R_1 = 0.532$ as in fig 3. Similarly the cathode is given $s = s_\epsilon \cong v_\epsilon^{3/4}$ and its distance from ideal cathode is $h_1 \cong R_1 v_\epsilon^{3/4}$. Outside beam region, anode shape is determined by Re $v_c(w) = v_a$ where v_c

is the complex analytic extension of $v_r(s)$; cathode shape is similarly determined. The gap boundary is drawn at Im $v_c(w) = v_3$ so that a pure Neumann condition exactly holds there; typically $v_3 = \frac{1}{2}$.

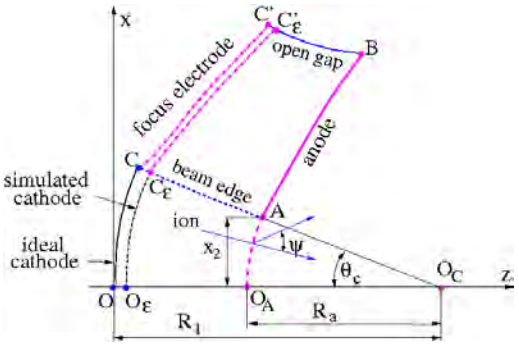

Figure 2: simulation geometry for closed anode and definition of angle ψ for open anode systems

2.2 The anode lens

The effect of a small hole in a anode is given in the thin lens approximation by the well known Davisson-Callbick formula[2, 5], which assumes as known the gradients $v_{,s}^-$ and $v_{,s}+$ on both sides of anode before the hole is drilled (minus refers to the gradient in the gap), which may be different. After hole formation, potential rearranges so that gradient is continuous, and this causes a lateral force (as a kick) of the ion which is so deviated by an angle ψ, see fig 2. Since ψ should vanish at $\ell = 0$ we can write

$$\tan\psi = c_1\ell + c_2 \mathrm{sign}(\ell)\ell^2 + c_3\ell^3 + O(\ell^4) \quad (7)$$

The Davisson-Callbick formula states $c_1 = \{v_{,s}^- - v_{,s}^+\}/(2v_a)$; some corrections may arise due to anode thickness; formula stays valid even with space charge, even if field gradient values change[6]. Notwithstanding several attempts[13], no simple formula is known for c_3; second order term, apparently suppressed by symmetry, was here written for future fitting purposes.

In the diode case, $v_{,s}^+ = 0$ since the drift tube is a field free region; before anode, the angle of ion flow with respect z axis is $\chi^- = -\ell$; after anode this angle becomes $\chi = \chi^- + \psi$. Neglecting all ℓ^2 terms in 7 the exit angle is

$$\chi = \ell\left[-1 + \frac{v_{,s}(s_a)}{2v(s_a)}\right] \quad (8)$$

At about $s_a = 0.630$ square bracket factor is zero, so that linear theory prediction is a parallel beam after anode; its validation will be preliminarily discussed in section 4.

3 Simulations for closed anode diodes

Validation test will consist in solving eq. 3 numerically in the fig 2) geometry with Comsol Multiphysics[14], and later by calculating the ion trajectory with post processing and verifying that they follow eq 4 flow lines within 4.5 digit precision. Reaching such a precision is remarkable but requires a careful specification of the geometry and of the simulation convergence, as explained in the following, pointing out the necessary conditions for a precise simulation.

a) First of all, series eq. 6 is calculated to 19-th order with a standard symbolic manipulation program[15], and the pertinent lines of fig 2 are written on ASCII files, for maximum flexibility of interchange. Each line consists of $2N + 1$ points, for each point we list z, x, Re v_c, Im v_c, s and ℓ.

When read by Comsol Multiphysics environment[14], line representation is changed to N circular arcs; arcs joins exactly; the angle discontinuity of the tangent from one arc to the other is usually negligible, since points were not equally spaced on the lines, but they were spaced closer near special points, in particular the junction C' of cathode, focus electrode and beam edge.

b) Note that at $v = 0$ equation 3 is singular, where $j_e(\ell) \neq 0$. The $v = 0$ line (ideal cathode) is so excluded by simulation domain, but furthermore we have to request that at the simulated cathode $v = v_\epsilon$ the mesh size h is about or smaller then $h_1 = R_1 v_\epsilon^{3/4}$, the distance between these cathodes.

When mesh size h does not satisfy this requests, we note for future reference that it convenient to temporarily modify eq 3 into

$$\triangle_z v = \frac{4C(z,x)}{9\sqrt{\sqrt{v^2 + (c_2)^2}}} \frac{j_e(\ell)}{R_1^2} \quad (9)$$

where cut-off c_2 is mesh dependent $c_2 > (h/R_1)^{4/3}$; so singularity is displaced where $v = \pm ic_2$, whose distance from cathode lines is about or greater than h. Note that

$C = 1/R$ with $R = ((z - R_1)^2 + x^2)^{1/2}$, thanks to eq 4 form.

c) To initialize v it is first convenient to solve eq 9 with $j_e = 0$, that is the Laplace equation. As a second step, eq. 9 is solved with a adequate cutoff $c_2 = \max(10^{-5}, (h/R_1)^{4/3})$. Finally (if mesh is adequate), eq 9 with $c_2 = 0$ is solved; since final result satisfies $v > v_\epsilon$, eq. 9 with $c_2 = 0$ and eq. 3 are equivalent. This also avoid both risks of producing imaginary values or encountering a singular Jacobian during solver iteration.

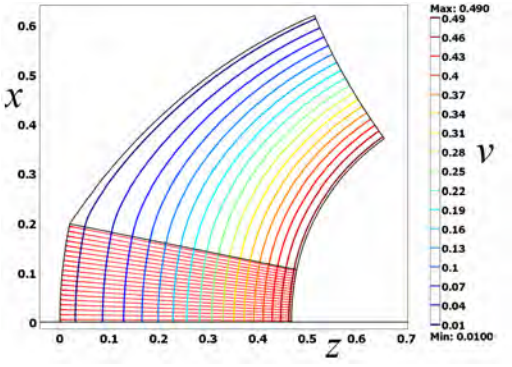

Figure 3: Equipotential for the closed anode with $v_a = 0.499$

3.1 results

In simulations, we take $R_1 = 1$ for simplicity; a typical results is shown in fig 3. The expected and calculated exit radius of test particles agrees better than 4 digit precision (5 digits for most particles). Some preliminary calculation with perturbation $j_e \neq 1$ to current density were published elsewhere[16].

4 Open anode diodes

To describe this geometry we need to introduce a few more parameters, as marked on fig 4. First of all, the anode hole half width h_a must surpass the unperturbed beam size at anode x_a by some factor, to allow some safety margin for the beam passage; in our simulation we specify the factor $F_\ell = \ell_a/\ell_1$ between the angle of the aperture ℓ_a and the angle of unperturbed beam ℓ_1 (as seen from point O_C); by trial and error, $F_\ell = 1.4$ s adequate in our case. Second we need to specify the exit plane position $z = R_4$ so that field gradient $v_{,z}$ is negligible there as compared $v_{,z}(s_a)$; this request $w(z = R_4) - s_a \gg \ell_a$ (considering the typical diffusion of field in apertures) or to give a firm bound $R_4 > z(w = s_a + \ell_a)$. Moreover diffusion of electric field is affected by the drift region half width r_d, which also need to be specify. On the other side $R_4 < R_1$ to exclude the point O_C from simulation.

In our example, taken $R_1 = 1$ as unit measure, we set $r_d = 0.25$ and $\ell_1 = 0.2$, which implies $\ell_a = 0.28$ and the limit $R_4 > 0.6$; we set $R_4 = 0.76$, which corresponds to $s_4 = w(z = R_4) = 1.42$. Moreover anode must have some finite thickness, so that we set curvature radius R_3 of the anode inner face as $R_a - 0.05$, where R_a defined in previous section is about the radius of outer face; we also chamfer the inner face edge.

In fig 4.a (real geometry) we thus determined all position except for the beam edge: motivation for use of transformation and moving mesh for our numerical solution is illustrated 4.b and c. Note that the simple theoretical guess for beam edge, based on the anode lens formula (dashed) gives a parallel beam at exit for this case (dashed line); a more prudent expectation, based on sparser experiments [2], considers a slightly divergent beam. Figure 4.b is purely the mapping of fig 4.a with eq. 4. Note that parallel beam $x = x_a$ is now a curved dashed line, given by $\ell = \text{asin}(x_a \text{e}^s)$; similarly drift tube $x = r_d$ face is now $\ell = \text{asin}(r_d \text{e}^s$. The exit line is now also a curved lime given $\ell = \text{acos}(r_5 \text{e}^s)$ with $r_5 = 1 - (R_4/R_1) = 0.24$ in our example. Figure 4.c coincides with 4.b for the metal parts, which must not move; but we change the beam region to a rectangle $[0, s_4] \times [0, \ell_1]$; we also rectify the exit boundary; this plane (Z, X) is reference plane for the moving mesh application 'ale'; in this plane, the trajectory of a particle is simply $X(Z) = \ell_i$ where $\ell = \ell_i$ was the starting coordinate at cathode.

The transform from reference frame to the spatial frame (z, x) (which is figure 4.a) needs to be defined in the following mode. On metal walls and cathode, transform is fixed and given $z + ix = w^{(-1)}(Z + iX)$; the application request to specify a deformation (not a transform), so actual input is $\text{d}z = z_n(Z, X) - Z$ and $\text{d}x = x_n(Z, X) - X$ where z_n and x_n are names of external function names. In beam region, we map point (Z, X) into $(z_M(Z; \ell_i), x_M(Z; \ell_i))$ where $\ell_i = X$;

moreover z_M and x_M are computed from motion equation. At exit plane $\mathrm{d}x$ is not assigned and $\mathrm{d}z = R_4 - Z$. Inside vacuum region, mesh deformation is free.

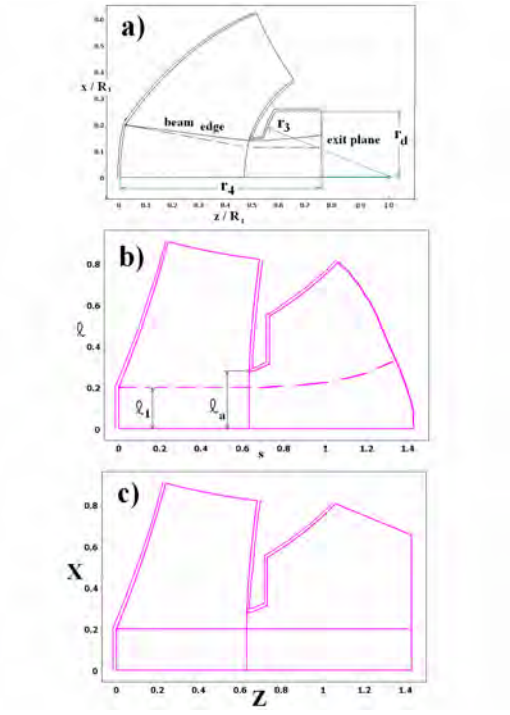

Figure 4: Open anode a) the real geometry in zx plane; electrode and cathode walls marked with double line; beam edge may move (theoretical predicted position is the dashed line); b) transform to w plane, with w defined by eq 4; c) fixed geometry ZX; here beam edge is made into a straight line, and exit plane into an open polygon)

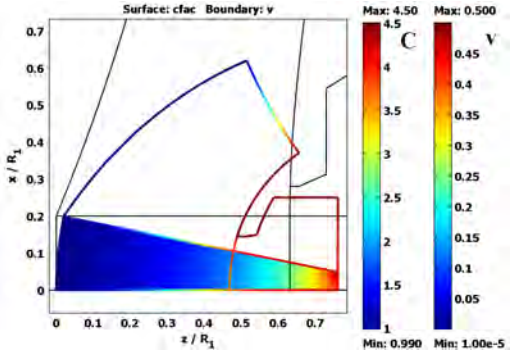

Figure 5: The convergence factor $C(z,x)$ at the $i_t = 0$ iteration; its definition domain is the beam area, at this stage a wedge spaced region. Real geometry (thick lines) and undeformed geometry (thinner lines)

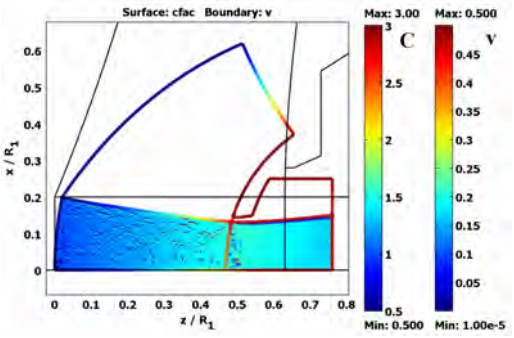

Figure 6: As fig 5, but for $i_t = 1$ (first iteration)

4.1 Iteration results

At code begin iteration $i_t = 0$, the motion maps z_M and x_M can be initialized arbitrarily; the simpler choice is not to use the anode lens correction at all and to set them according to eq. 4. First z and x are calculated on the Z, X mesh; then Poisson eq. 9 is solved in this (z, x) geometry and with three steps of item c) in previous section; the convergence factor map be computed from motion map, or for saving programming effort by the approximation

$$C(z,x) = 1/\sqrt{(x_{,X})^2 + (x_{,Z})^2} \qquad (10)$$

Figure 5 show computed $C(z,x)$, and how beam was approximated at this stage.

In first iteration $i_t = 1$ the motion equations

$$z_{,\lambda\lambda} = v_{,z} \quad , \quad x_{,\lambda\lambda} = v_{,x} \qquad (11)$$

where λ is a scaled time are solved (for $N = 20$ test particles $i = 1, \ldots, N$) with a leapfrog method, calling 'postinterp' to evaluate the four variable $v_{,z}$, $v_{,x}$, Z and X at current z, x positions. Data for λ, z, x, Z, x are recorded each time 'postinterp' is called. For each test particle i, as matter of fact, Z grows in a monotonic way with λ; therefore map $x_M(Z; \ell_i)$ is easily computed by 'interp1' at any desired Z.

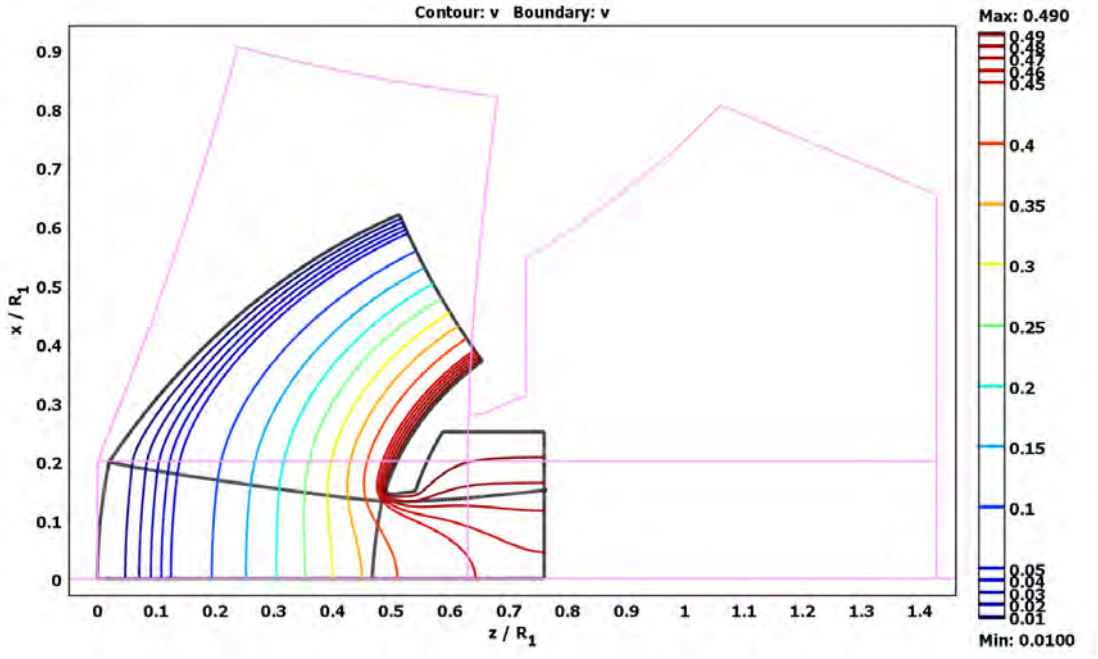

Figure 7: Equipotential contout lines of v; boundaries are also shown for real geometry (thicker lines) and undeformed geometry (thinner lines)

Note that we choose $\ell_i = (i - \frac{1}{2})\theta_c/N$, so that beam edge $\ell_i = \theta_c$ is not directly computed by leapfrog; we recover beam edge from

$$x_M(Z;\theta_c) = \tfrac{3}{2}x_M(Z;\ell_N) - \tfrac{1}{2}x_M(Z;\ell_{N-1}) \quad (12)$$

(this choice has some advantages and disadvantages) and a similar extension of z_M. Moreover to simplify programming, only beam edge position is loaded back to application 'ale', leaving the interpolation inside beam to the Comsol Multiphysics free moving mesh algorithm. After $C(z,x)$ is calculated from eq. 10 and updated mesh, as shown in fig 6, solution for potential v is updated, using of course the previous v as initial guess for nonlinear solver; only the third step of mentioned procedure of item 'c' is repeated. This completes iteration.

An overview of complete results is shown in fig 7. Note that beam edge has moved very near to anode hole edge, proving that deviation from line converging flow is substantial. This happens because we simulated a relatively large cathode $\theta_c = 0.2$ rad, which forces us to use a large aperture $\ell_a = 0.28$, which is comparable to gap size $s_a = 0.63$ and agrees with trends measured elsewhere[2].

Figure 7 show the ray trajectory at several i_t; only 3 iterations were enough to obtain convergence to final result, which is a very remarkable property of this moving mesh algorithm. Probably convergence can made even faster with a better z_M initial choice, if this is worthwhile. Note also beam aberration is much smaller at converged result than is for $i_t = 1$.

At this initial development stage there are of course some open questions. First of all, the final beam divergence is large (110 mrad in this example), which make us to reconsider the cathode-anode gap design; in particular increasing length s_a and voltage v_a. Moreover, note that, due to the triangular mesh used also in the beam region some local fluctuations in C values are apparent; provided that average fluctuation is near zero, this has scarce effect on the whole beam profile. Work on refining mesh and on fitting result with eq. 7 formula is well in progress.

In summary, the moving mesh is a powerful tool to model a laminar beam, since this flow can be mapped to a rectangle. Moreover the cathode and electrode shape which in real space have rather warped shapes may be mapped to simpler shapes by similar maps. After solving the Poisson equation for the electric field, only the trajectories of few ions

need to be computed, in order to update the map from the rectangular beam representation to its real shape. Iteration is very rapidly converging. The numerical solution so found reproduces faithfully the laminar beam assumption, and is of great value to verify (and eventually correct) the theoretical predictions and design rules.

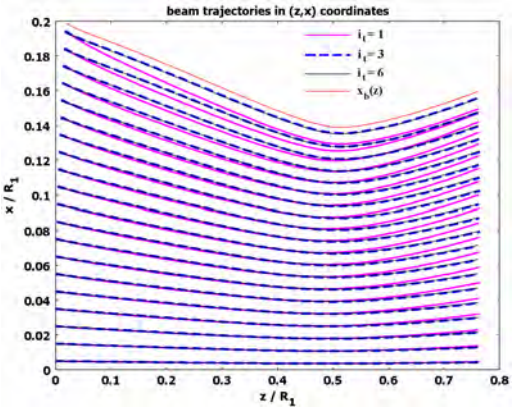

Figure 8: Trajectories at several iteration count i_t; the $i_t = 1$ result (thick solid line) has visible aberrations of the 19-th and 20-th rays, which reduces in the $i_t = 3$ result (thick dashed line) and in the $i_t = 6$ result (thin line), practically superposed; other iteration not shown for graph readability. Outer envelope $x_b(z)$ from eq. 12 is also shown.

References

[1] R. J. Pierce, *Theory an design of electron beams*, Van Nostrand, Princeton, 1954 (2nd edition)

[2] G. R. Brewer "High-intensity electron guns" in *Focusing of Charged Particles* (ed. A. Septier, Academic Press, Orlando, 1967) vol. 2, p 23-72

[3] I. Langmuir and K. Blodgett, *Phys Rev.*, **22** , 347 (1923)

[4] W.E. Danielsom, J. L. Rosenfeld, J. A. Saloom, A detailed analysis of beam formation with electron guns of the Pierce type, Bell System Tech. J. **25**, 375 (1956)

[5] G. J. Davisson and C. J. Callbick, *Phys. Rev. 42*, 580 (1932)

[6] J. R. Coupland, T. S. Green, D. P. Hammond, and A. C. Riviere, *Rev. Sci. Instrum.*, **44**, 1258, (1973).

[7] I. Chavet, R. Bernas, A study of the beam divergence in an electromagnetic isotope separator Nuclear Instruments and Methods, **47**, 77 (1967).

[8] I. Chavet, M. Kanter, M. Menat, The divergence profile of a wedge-type ion beam, Nuclear Instruments and Methods, **153**, 317 (1978).

[9] G. D. Alton and H. Bilheux, Rev. Sci. Instrum. 75, 1431 (2004);

[10] H. P. L. de Esch, R. S. Hemsworth, and P. Massmann, SINGAP: The European concept for negative ion acceleration in the ITER neutral injectors, Rev. Sci. Instrum., **73**, pp1045-1047 (2002)

[11] O. B. Morgan, G. G. Kelley, and R. C. Davis Technology of Intense dc Ion Beams Rev. Sci. Instrum. 38, 467 (1967)

[12] M. Cavenago, P. Veltri, F. Sattin, G. Serianni, V. Antoni, *IEEE Trans. on Plasma Science*, **36**, pp 1581-1588 (2008)

[13] C. K. Birdsall, Aperture Lens Formula Corrected for Space Charge in the Electron Stream, IRE Trans. Electron Devices, 132 (1957)

[14] *Comsol Multiphysics 3.5* or higher version, see also http://www.comsol.eu

[15] Mathematica 5.2 (or higher versions), http://www.wolfram.com/

[16] M. Cavenago, Ion extraction system optimization, AIP Proceedings of ION-BEAMS 2012, 6-8 June 2012, Legnaro (eds R. A. Ricci, V. Rigato, in press)

[17] P. Spadtke, Rev. Sci. Instrum., **75**, 1643 (2004)

[18] R. Becker, Rev. Sci. Instrum. 75 (2004), 1687

[19] R. F. Welton, M. P. Stockli, J. Boers, R. Rauniyar, R. Keller, J. W. Staples and R. W. Thomae, Rev. Sci. Instrum. 73 (2002), 1013